

Smale – Williams solenoids in autonomous system with saddle equilibrium

## Smale – Williams solenoids in autonomous system with saddle equilibrium

S. P. Kuznetsov,<sup>1</sup> V. P. Kruglov,<sup>1,2, a)</sup> and I. R. Sataev<sup>1, b)</sup>

<sup>1)</sup>*Kotel'nikov's Institute of Radio-Engineering and Electronics of RAS, Saratov Branch, Zelenaya 38, Saratov 410019, Russia*

<sup>2)</sup>*Institute of Electronic Engineering and Instrumentation, Yuri Gagarin State Technical University of Saratov, Politekhmicheskaya 77, Saratov 410054, Russia*

(Dated: 11 December 2020)

We construct an autonomous low-dimensional system of differential equations by replacement of real-valued variables with complex-valued in a self-oscillating system with homoclinic loops of a saddle. We provide analytical and numerical indications and argue that the emerging chaotic attractor is uniformly hyperbolic chaotic attractor of Smale – Williams type. The four-dimensional phase space of the flow consists of two parts: a vicinity of a saddle equilibrium with two pairs of equal eigenvalues, where the angular variable undergoes a Bernoulli map, and a region, which ensures that the trajectories return to the origin, without angular variable changing. The trajectories of the flow approach and leave the vicinity of saddle equilibrium with the arguments of complex variables undergoing a Bernoulli map on each return. That makes possible the formation of the attractor of Smale – Williams type in Poincaré cross-section. Our model in essence resembles complex amplitude equations governing the dynamics of wave envelopes or spatial Fourier modes. We discuss the roughness and generality of our scheme.

**The concept of uniformly hyperbolic attractors as geometrical representation of deterministic chaos was born during the *hyperbolic revolution* at 1960s-1980s in pioneering works of Smale, Anosov, Williams, Plykin and others. Uniformly hyperbolic chaotic attractors are the simplest ones from geometrical point of view in the sense that they allow full and rigorous mathematical description. But the most importantly, they are rough objects, insusceptible to parameter variations or noise. There was hope that uniformly hyperbolic attractors would appear naturally in various physical problems, like turbulence. But it turned out that chaotic attractors in most of the situations do not belong to this class. L.P.Shilnikov and D.V.Turaev<sup>1,2</sup> in series of works about the so-called blue sky catastrophe gave the first example of bifurcation leading to the possibility of appearance of hyperbolic attractors of Smale–Williams type in Poincaré section of continuous-time systems. Recently a breakthrough happened with physically reliable examples of systems with Smale – Williams solenoids and Plykin-type attractors. These examples are realistic with some of them have been implemented in experiments, but they are somewhat complicated for mathematical analysis. In the context of this work we consider the occurrence of an attractor of Smale – Williams type in a relatively simple system of ordinary differential equations. We report the simplest to our knowledge 4-dimensional autonomous system of differential equations with attractors of Smale – Williams type in Poincaré cross-section, that allows very clear understanding of phase space transformations. We consider the uncovered arrangement of Smale – Williams attractor formation to be general for a wider bunch of autonomous systems.**

### I. INTRODUCTION

Uniformly hyperbolic strange attractors are pure mathematical form of chaos<sup>3-9</sup>. They consist exclusively of saddle trajectories. For discrete maps the tangent space of any point of saddle orbit splits into two invariant subspaces: expanding and contracting. Contracting (expanding) subspaces consist of vectors with exponentially decreasing norms in forward (backward) time evolution. Rates of decrease are bounded and far from zero at every point of attractor. An arbitrary small perturbation vector of a saddle trajectory is a linear combination of vectors, belonging to these subspaces. The set of trajectories, that asymptotically converge to the saddle trajectory in forward (backward) time, is its stable (unstable) manifold. Stable (unstable) manifolds of every trajectory of uniformly hyperbolic attractor have the same dimension. Stable and unstable manifolds of every trajectory on hyperbolic attractor are only transversal to each other.

The uniformly hyperbolic attractors have remarkable attributes due to their structure<sup>6,9</sup>. Most importantly, uniformly hyperbolic attractors are structurally stable (or rough): small perturbations do not destruct them. This feature is not common to the most of chaotic attractors that appear in physical problems. Usual examples of chaotic attractors are so-called quasiattractors<sup>10</sup> which contain attractive periodic trajectories due to non-transversal intersections of stable and unstable manifolds, and thus are not genuine strange attractors<sup>7,11</sup>. Quasiattractors in contrast to genuine strange attractors are not structurally stable. Much less common are pseudo-hyperbolic genuine attractors<sup>7,12</sup>, which are structurally stable. The famous example of pseudohyperbolic attractor is the Lorenz attractor<sup>13-17</sup>, which appears in three-dimensional phase spaces with saddle equilibrium. The first physical system involving Lorenz attractor originates in hydrodynamics<sup>18</sup> — it is a low-dimensional Galerkin approximation of the convection problem in the layer of fluid heated from below.

Smale – Williams solenoid is a textbook geometrical example<sup>4,6,7,9,19</sup> of uniformly hyperbolic attractor. It appears

<sup>a)</sup>Electronic mail: kruglovyacheslav@gmail.com

<sup>b)</sup>Electronic mail: sataevir@gmail.com

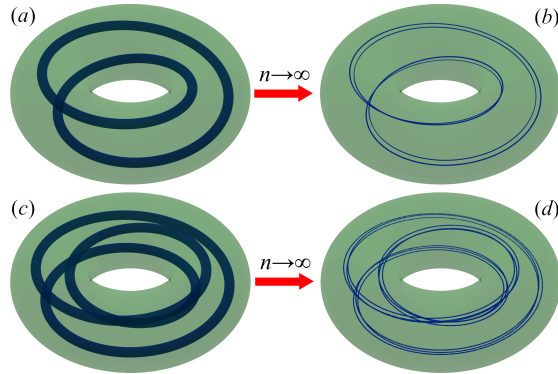


FIG. 1. (a) The toroidal domain in phase space (green) and its image (blue) by the map (1) with factor  $m = 2$ , (b) the image after many iterations tends to Smale – Williams solenoid with factor 2, (c) and (d) panels show the same procedure with expansion factor  $m = 3$ . The images were plotted by numerical iterations of map (1). The parameter values of (1) are  $\alpha = 0.125$ ,  $\varepsilon = 0.25$ .

as an attracting limit set of the special type of maps in phase space of dimension at least 3. The map should by one iteration expand a toroidal domain in angular direction  $m = 2, 3, \dots$  times, but strongly compress in other directions and fold inside the initial toroid. The exact map can be chosen in a following way:

$$\begin{aligned} \theta_{n+1} &= m\theta_n \pmod{2\pi}, \\ r_{n+1} &= 1 + \alpha(r_n - 1) + \varepsilon \cos \theta_n, \\ z_{n+1} &= \alpha z_n + \varepsilon \sin \theta_n, \end{aligned} \quad (1)$$

where  $\theta$  is the angular variable,  $\alpha$  and  $\varepsilon$  are some parameters less than 1, and  $m$  is an integer expansion factor. The first equation in (1) is called Bernoulli map, and it is the cause of chaotic dynamics on Smale – Williams solenoid. Instead of explicit form of map with separate equation for angular variable one can visualize a transformation in Cartesian coordinates:  $X_n = r_n \cos \theta_n$ ,  $Y_n = r_n \sin \theta_n$  and  $Z_n = z_n$ . Thus the angular variable  $\theta$  can be defined as the argument of complex variable  $X + iY$ . The visualizations of Smale – Williams solenoids construction with expansion factors 2 and 3 are pictured on Fig. 1.

The first example of system, governed by differential equations, with the attractor of Smale – Williams type in Poincaré cross-section was proposed by Kuznetsov<sup>20</sup>. The system is composed of two nonautonomous van der Pol oscillators with natural frequencies differing by factor 2. Due to counterphase periodic modulation of control parameter both oscillators enter and exit self-oscillations regime alternately. The excitation transmits from one oscillator to another with help of special nonlinear terms in such a way, that the phase of oscillations undergoes Bernoulli map on each period of modulation. We refer to this arrangement of nonlinear interaction between subsystems as phase manipulation. This approach turned out to be fruitful, since many other examples were subsequently proposed with the Smale-Williams attractor based on it, some

of them are autonomous systems<sup>21</sup> and even spatially extended<sup>22</sup> and governed by PDE<sup>23</sup>. We do not stray away from phase manipulation approach too. Regarding the Kuznetsov system, the hyperbolic nature of its attractor was approved numerically using cone criteria<sup>24</sup> and rigorously confirmed by computer-assisted proof<sup>25</sup>. It was also implemented as radio-electronic circuit<sup>26</sup>.

In the present paper we present another way to construct the system with attractor of Smale-Williams type and provide numerical evidences of its hyperbolic nature. The equations are derived by replacement of real-valued variables with complex-valued in a self-oscillating system with homoclinic loops of a saddle. The homoclinic bifurcation of such type was studied by L.P.Shilnikov<sup>27</sup>. Section II describes the construction of flow governed by relatively simple equations with an attractor of Smale – Williams type. The geometrical structure of phase space allows simple description of transformations. Section III contains some numerical results concerning the attributes of uniformly hyperbolic attractors. Appendix proposes some substantial modifications of the model, that keep or destroy the hyperbolic structure of chaotic attractor.

## II. THE CONSTRUCTION

Let us start with linear system of ordinary differential equations:

$$\begin{aligned} \dot{z} &= w, \\ \dot{w} &= z + aw, \end{aligned} \quad (2)$$

where  $z = x + iy$  and  $w = u + iv$  are complex variables and  $a$  is real parameter. The system (2) is a composition of two identical disjunct linear systems with real variables, one can rewrite it in four-dimensional vector–matrix form:

$$\frac{d}{dt} \begin{bmatrix} x \\ u \\ y \\ v \end{bmatrix} = \begin{bmatrix} 0 & 1 & 0 & 0 \\ 1 & a & 0 & 0 \\ 0 & 0 & 0 & 1 \\ 0 & 0 & 1 & a \end{bmatrix} \cdot \begin{bmatrix} x \\ u \\ y \\ v \end{bmatrix}$$

The system (2) has a saddle equilibrium at the origin with two identical negative characteristic exponents  $\lambda_1 = \lambda_3 = \frac{1}{2}(a - \sqrt{a^2 + 4})$  and two identical positive characteristic exponents  $\lambda_2 = \lambda_4 = \frac{1}{2}(a + \sqrt{a^2 + 4})$ . Thus the saddle has two-dimensional stable and unstable invariant manifolds without distinguished “strong” or “weak” subdirections on them.

Since the system splits into two identical independent linear two-dimensional subsystems, the general solution of (2) may be presented in a form

$$\begin{aligned} z(t) &= A e^{\lambda_1 t} + B e^{\lambda_2 t}, \\ w(t) &= \lambda_1 A e^{\lambda_1 t} + \lambda_2 B e^{\lambda_2 t}, \end{aligned} \quad (3)$$

where complex constants  $A$  and  $B$  are defined by initial conditions. If  $|B| \ll |A|$ , then the initial condition is close to stable manifold and the trajectory comes near to the saddle. The argument of complex  $A$  defines the “angle of incidence” of the

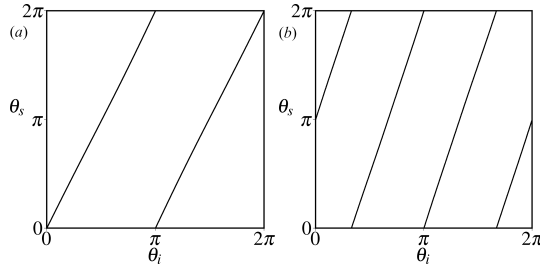


FIG. 2. “Scattering” diagrams at  $a = -0.68$ ,  $\varepsilon = 0.1$ , (a)  $m = 2$ , (b)  $m = 3$ . The initial angles  $\theta_i$  vary from 0 to  $2\pi$  and “scattered” angles spread over this interval  $m$  times.

trajectory on the saddle equilibrium in the  $z$  complex plane and the argument of  $B$  defines the “scattering angle” of the trajectory.

We add a small nonlinear perturbation to equations (2):

$$\begin{aligned} \dot{z} &= w, \\ \dot{w} &= z + aw + \varepsilon w^m, \end{aligned} \quad (4)$$

where  $\varepsilon$  is small parameter and  $m$  is positive integer.

If  $\varepsilon = 0$  and the initial condition belongs to the stable manifold ( $B = 0$ ), then the solution is  $z(t) = A e^{\lambda_1 t}$ ,  $w(t) = \lambda_1 A e^{\lambda_1 t}$ . Such trajectory tends exactly to the saddle equilibrium (let us remind that  $\lambda_1 < 0$ ). If the value of parameter  $\varepsilon \neq 0$ , but is small, the trajectories from the same initial point would miss the saddle, but come close to it. We argue that the saddle equilibrium in system (4) “deflects” close trajectories in such way, that “incident” angles transform to “scattering” angles according to Bernoulli type map. Let us first demonstrate this by numerical visualization and then support it by perturbation analysis.

The plane tangent to stable manifold at the saddle point is defined by two unit eigenvectors  $\hat{e}_1$  and  $\hat{e}_2$ . If we take the initial point in the plane spanned by these two vectors at unit distance from the saddle  $\hat{e}_1 \cos \theta_i + \hat{e}_2 \sin \theta_i$ , where  $\theta_i$  is arbitrarily chosen angle, then for small enough  $\varepsilon$  values  $\theta_i$  will define the angle, at which the trajectory will fall on the saddle in the  $z$  complex plane. We vary the angle  $\theta_i$  from 0 to  $2\pi$  and simulate numerically the “scattering” of trajectories on the saddle catching them later at unit distance from the origin (the concrete numerical values for parameters of numerical simulations you can find in the footnote<sup>28</sup>). We plot the “scattered” angles  $\theta_s = \arg z$  vs. initial ones  $\theta_i$ . Fig. 2 shows transformation of trajectories directions near the saddle at  $a = -0.68$  (surely one can choose the parameter  $a$  value arbitrarily to some extent). The “scattering” diagrams for  $m = 2, 3$  correspond to Bernoulli type map.

Now let us support our numerical results by perturbation analysis of (4) for small  $\varepsilon$ .

Our analysis (without pretensions to be rigorous) is based on suggestion that for small enough  $\varepsilon$  values the dynamics in the close vicinity of the saddle may be regarded as linear, then the trajectory “scattering” angle value will be defined by the complex amplitude of the unstable mode  $B$  (see (3)), that the

system would pick up at the “falling” part of the trajectory. Hence, our goal is to get the estimation for this amplitude.

We take the perturbed solution in the form

$$\begin{aligned} z(t) &= A e^{\lambda_1 t} + \varepsilon B(t) e^{\lambda_2 t}, \\ w(t) &= \lambda_1 A e^{\lambda_1 t} + \varepsilon (\lambda_2 B(t) + \dot{B}(t)) e^{\lambda_2 t}. \end{aligned} \quad (5)$$

The initial conditions for perturbation function are  $B(0) = 0$ ,  $\dot{B}(0) = 0$ .

Substituting the ansatz (5) to the equations (4) we obtain equation for  $B$ :

$$\ddot{B} + (2\lambda_2 - a)\dot{B} = (\lambda_1 A e^{\lambda_1 t} + \varepsilon (\lambda_2 B(t) + \dot{B}(t))) e^{\lambda_2 t})^m e^{-\lambda_2 t} \quad (6)$$

The term with small parameter  $\varepsilon$  enters with a rapidly growing factor. But we are only interested in the “falling” section of the trajectory, on which the damped mode dominates. The damped mode and the growing unstable mode become comparable only in the nearest to the saddle segment of the trajectory, where, according to our suggestion, dynamics is close to linear. Then, discarding the corresponding part of the nonlinear term, we obtain an equation for the function  $B$  on the “falling” part of the trajectory

$$\ddot{B} + (2\lambda_2 - a)\dot{B} = \lambda_1^m A^m e^{(m\lambda_1 - \lambda_2)t}. \quad (7)$$

In fact, this is equation for the evolution of the germ of the unstable mode on the “falling” part of the trajectory under the influence of damping stable mode, when the latter dominates. The solution for  $B(t)$  consists of solution of homogeneous equation and a term due to external force. With initial conditions  $B(0) = 0$ ,  $\dot{B}(0) = 0$  it is

$$\begin{aligned} B(t) &= \frac{\lambda_1^m A^m \lambda_2}{(m-1)(\lambda_1 - \lambda_2)} e^{(\lambda_1 - \lambda_2)t} + \frac{\lambda_1^m A^m}{(m\lambda_1 - \lambda_2)(\lambda_1 - \lambda_2)} \\ &\quad - \frac{\lambda_1^m A^m \lambda_2}{(m-1)(m\lambda_1 - \lambda_2)} e^{(m\lambda_1 - \lambda_2)t}, \end{aligned} \quad (8)$$

where the Vieta’s formulas  $\lambda_1 + \lambda_2 = a$ ,  $\lambda_1 \lambda_2 = -1$  were used. If we substitute (8) into (5), then it turns out that the first term is a small, of the order of  $\varepsilon$ , correction to the amplitude of the damped mode  $A$ . The second and third terms describe the evolution of the germ of an unstable mode. By the time the trajectory approaches the origin, the complex argument of the amplitude  $B$  will be determined by the complex argument of the quantity  $B \propto \lambda_1^m A^m$  and the argument of variable  $B$  becomes  $m \arg \lambda_1 A$ .

The argument of  $z$  transforms from  $\theta_i = \arg z(0) \approx \arg A$  to  $\theta_s = \arg z(\tau) \approx m \arg \lambda_1 A$ :

$$\theta_s = m\theta_i + C \pmod{2\pi}, \quad (9)$$

where  $C = 0$  or  $\pi$  depending on  $m$  even or odd. This is the Bernoulli mapping. We have obtained this result in the first-order approximation for the part of the trajectory, approaching the saddle near the stable manifold. It corresponds to our numerical experiments with the “scattering” of the trajectories near the saddle (Fig. 2).

In the described setup the trajectories approach the saddle no more than once and flee to infinity after the “scattering”. To construct a chaotic flow we should introduce a mechanism of reinjection of trajectories into the vicinity of the saddle. A situation near a formation of homoclinic loop of the saddle seems to be appropriate to realize the required mechanism.

Let us consider the following two-dimensional model of self-oscillator:

$$\begin{aligned}\dot{x} &= u, \\ \dot{u} &= (1-x^2)x + [L - (1-x^2)^2]u,\end{aligned}\quad (10)$$

where  $x$  and  $u$  are real variables, and  $L$  is the control parameter of Andronov – Hopf bifurcation. The system has a saddle equilibrium at  $(0, 0)$  and two foci at  $(\pm 1, 0)$ . The foci lose stability at  $L = 0$  and two stable limit cycles arise at  $L > 0$  (Fig. 3a). At  $L \approx 0.3197$  the limit cycles glue into bi-asymptotic trajectories of the saddle<sup>27</sup> (Fig. 3b), at  $L > 0.3197$  a limit cycle forms surrounding all three equilibria (Fig. 3c).

Let us couple two identical systems (10) in an unusual way:

$$\begin{aligned}\dot{z} &= w, \\ \dot{w} &= (1-|z|^2)z + [L - (1-|z|^2)^2]w.\end{aligned}\quad (11)$$

New variables  $z = x + iy$ ,  $w = u + iv$  are complex,  $u = \dot{x}$ ,  $v = \dot{y}$ . The feedback and the restoring force have factor  $|z|^2 = x^2 + y^2$  instead of  $x^2$ , and depend on both oscillators. While we do not

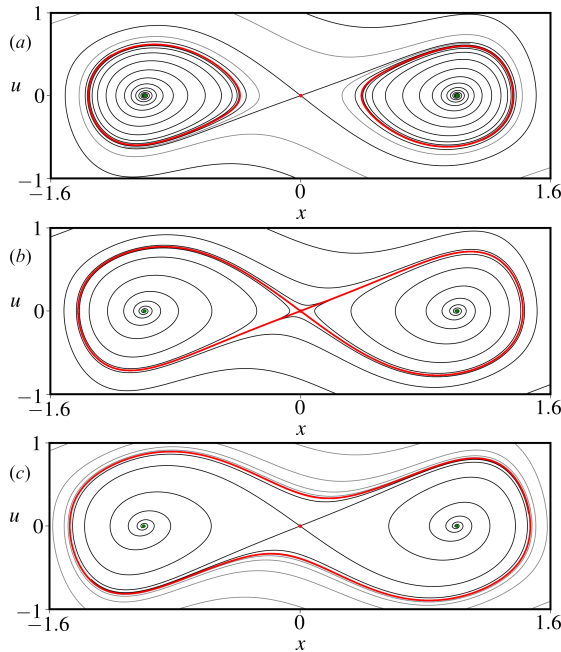


FIG. 3. (a)  $0 < L < 0.3197$ , (b)  $L \approx 0.3197$ , (c)  $L > 0.3197$ . Numerical solutions of equations (10). The limit cycles are colored red, saddle equilibrium is pointed red, foci are pointed green.

know of any actual physical example of system (11), it closely resembles complex amplitude reductions, describing wave envelopes or spatial modes in pattern formation distributed systems<sup>29</sup>. The saddle at the origin has two negative equal eigenvalues and two positive equal eigenvalues. Instead of two foci the introduced complexification brings a continuum of equilibria  $(e^{i\phi}, 0)$ , where  $\phi$  is any angle. Linearization of system (11) near the saddle is exactly system (2) with  $a = L - 1$ . If  $\arg z - \arg w = 0$  or  $\pi$ , then arguments remain constant and complex system (11) reduces to two-dimensional real amplitude system governed exactly by equations (10). Actually cases  $\arg z - \arg w = 0$  or  $\pi$  correspond to limiting at  $t \rightarrow \infty$  solutions, therefore phases tend to constant values. The important to our construction fact is that while the trajectories are far from the saddle, the arguments do not change.

The last step is to add small perturbation  $\varepsilon w^m$ :

$$\begin{aligned}\dot{z} &= w, \\ \dot{w} &= (1-|z|^2)z + [L - (1-|z|^2)^2]w + \varepsilon w^m.\end{aligned}\quad (12)$$

This model, in the  $m = 3$  case, was discussed for the first time in article<sup>30</sup>. One can imagine the phase space of system (12) composed of two parts: a vicinity of the saddle equilibrium, where trajectories “scatter” with angular variable undergoing Bernoulli map transformation, and a region, where trajectories revolve around the circle of equilibria with constant  $\arg z$  and  $\arg w$ . The trajectories successively visit these regions. In the next section we provide numerical evidence that the attractor of Smale – Williams type exists in Poincaré cross-section of (12).

### III. RESULTS OF NUMERICAL INVESTIGATIONS

Equations (12) were solved numerically with Runge – Kutta 4<sup>th</sup> order routine. Fig. 4a,b show portrait of the attractor in flow system (12) with expansion factor  $m = 2$ . Fig. 4a gives a projection on plane  $(\text{Re}z, \text{Im}z)$ . One can see, that typical trajectory changes the direction near the origin, and then moves radially forth and back almost straight. Fig. 4b demonstrates another projection  $(\text{Re}z, \text{Re}w)$ . Comparing panels (a) and (b) one can get an impression of trajectory behaviour in four-dimensional phase space. Outside the vicinity of the origin the trajectory moves close to one half of “figure-8” loop inside a narrow slice of space given by some angle  $\theta = \arg z$ . Close to the origin (but actually at some finite distance from the saddle) the trajectory turns to some different angle and bounces. To reveal quantitatively the transformation of angle we must construct numerically an appropriate Poincaré return map. Fig. 4c,d demonstrate the attractor in system (12) with expansion factor  $m = 3$ . The difference from the system with  $m = 2$  is more uniform distribution of the trajectories in phase space. Fig. 4e,f show portraits in projection on the plane of amplitudes  $(|z|, |w|)$ . In our simulations the trajectories never come arbitrarily close near the saddle equilibrium (at the parameter values corresponding to apparently uniformly hyperbolic attractor). To confirm this we have numerically evaluated

This is the author's peer reviewed, accepted manuscript. However, the online version of record will be different from this version once it has been copyedited and typeset. PLEASE CITE THIS ARTICLE AS DOI: 10.1063/1.50028921

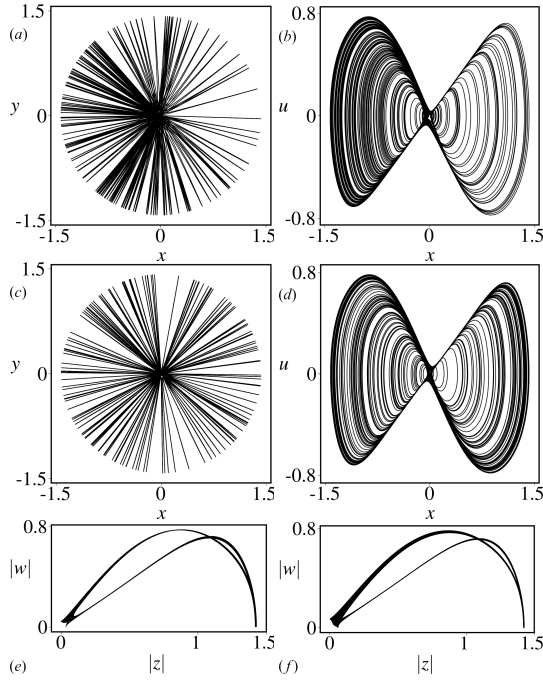


FIG. 4. Projections of attractor in flow system (12),  $L = 0.32$ ,  $\varepsilon = 0.02$ . Panels (a), (b) and (e) are for  $m = 2$ . Panels (c), (d) and (f) are for  $m = 3$ .

minimal distances  $\rho = \sqrt{|z|^2 + |w|^2} = \sqrt{x^2 + y^2 + u^2 + v^2}$  between the typical trajectories and the saddle equilibrium. Each time the minimal distance became less than previously obtained value, the new value had been appended to the stored data. Fig. 5a,b show dependencies of the minimal distances from time of simulation (in log-log scale) for  $m = 2$  and  $m = 3$ . The initial conditions had been picked such that at the beginning of the simulation the trajectory is far from the saddle:  $\rho(0) = 1$ . The minimal distance for  $m = 2$  converges to  $\rho_{min} \approx 0.0353013$ . The minimal distance for  $m = 3$  converges to  $\rho_{min} \approx 0.0370982$ .

We choose the cross-section surface  $S = |z|^2 - 1 = 0$  to construct the Poincaré map (for certainty the trajectory crosses it from negative to positive values of  $S$ ). Since the absolute values  $|z|$  are fixed on the cross-section, the variables of the map are  $\theta = \arg z$ ,  $u = \operatorname{Re} w$ ,  $v = \operatorname{Im} w$ , thus the transformation of the angular variable is explicit. Fig. 6a,c show iterations of argument  $\theta_{n+1}$  vs.  $\theta_n$  for versions of equations (12) with expansion factor  $m = 2$  and  $m = 3$ . The pictures are in agreement with Bernoulli transformation: the preimage interval of length  $2\pi$  (one turn around the circle) is mapped to the  $2m\pi$  interval, wound around a circle  $m$  times. The apparent splitting of the diagram Fig. 6a reflects the fractal structure of the attractor of Smale – Williams type (this is an approximate one-dimensional map defined on the coordinates of the empirical attractor; the main purpose of these illustrations is to demonstrate, that the mapping for the phase is everywhere

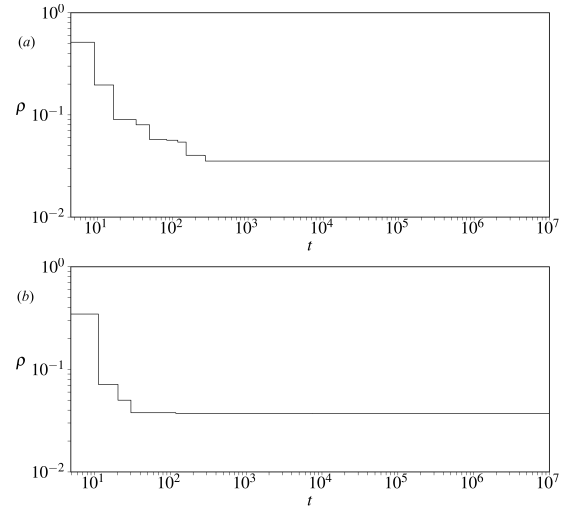


FIG. 5. The minimal distance  $\rho$  of the typical trajectory in flow system (12) from the saddle equilibrium vs. time of simulation (in log-log scale),  $L = 0.32$ ,  $\varepsilon = 0.02$ . Panel (a) is for  $m = 2$ . Panel (b) is for  $m = 3$ .

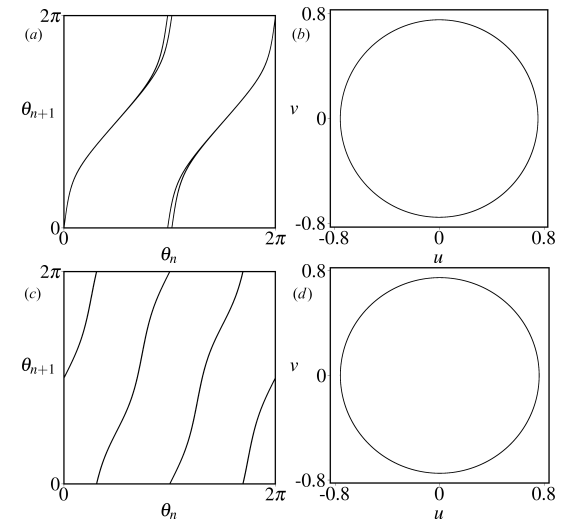


FIG. 6. Iterations of argument  $\theta_{n+1}$  vs.  $\theta_n$  (a,c) and the attractor of Poincaré map (b,d) of the system (12),  $L = 0.32$ ,  $\varepsilon = 0.02$ . Panels (a) and (b) are for  $m = 2$ . Panels (c) and (d) are for  $m = 3$ .

expanding). We have checked numerically, that the transformation of the angular variable is exactly  $m$  times stretching, continuous and monotonic. The routine is simple<sup>31–33</sup>. We split the  $2\pi$  interval into  $N$  pieces, iterate the map and accumulate the averages  $\Phi_k = \frac{1}{T_k} \sum_{n=0}^{T_k} e^{i\theta_n}$  of  $\theta_n$  values, that hit into the  $k$ -th interval,  $k \in [0, N]$  is the index of small interval,  $T_k$  is the hit count of small interval  $k$ . First we ver-

ify the absence of empty intervals after sufficiently long time of numerical simulation. If the hit count  $T_k$  of every interval is nonzero, the transformation is continuous. If all angular shifts  $\arg \Phi_{k+1} - \arg \Phi_k$  between neighboring intervals are positive, the transformation is monotonous. The final step is to calculate the sum  $M = \frac{1}{2\pi} \sum_{k=0}^{N-1} (\arg \Phi_{k+1} - \arg \Phi_k)$ , which is the expanding factor of the transformation. Our calculations confirm, that for Poincaré return map of the system (12) at  $L = 0.32$ ,  $\varepsilon = 0.02$ ,  $m = 2, 3$  transformation is continuous, monotonous and expanding in exactly  $M = m = 2, 3$  times. We clarify that our calculations are not rigorous mathematical proof, but rather a good way to distinguish the map of Bernoulli type in numerical data. Figures 6b,d show projections of Poincaré map attractor onto plane of variables  $u, v$  (cases  $m = 2$  and 3). Due to strong compression of the phase space in directions transversal to the angular coordinate the portraits of attractors look like very tight rings. The rates of expansion and contraction can be estimated with calculations of Lyapunov exponents.

The Lyapunov exponents were calculated by the usual algorithm<sup>34–36</sup> with Gram – Schmidt orthogonalization of perturbation vectors<sup>37</sup>. For parameter values  $L = 0.32$ ,  $\varepsilon = 0.02$  and  $m = 2$  (corresponding to Figures 6a,b) the Lyapunov exponents for trajectories of attractor of three-dimensional Poincaré map are  $\Lambda = \{0.537 \pm 0.001, -2.931 \pm 0.003, -3.827 \pm 0.001\}$ . The first Lyapunov exponent is positive. It is less than the Lyapunov exponent of the Bernoulli map  $\Lambda_{B_2} = \ln 2 \approx 0.693$ . Nevertheless, the numerical check of angular variable expansion, described above, confirms that topological factor is  $m = 2$ . We do not know the exact reason for the mismatch, but we suppose it might be explained by small perturbation of the angle transformation, which does not violate overall twofold expansion. In this case the calculation of topological expansion factor has become very handy. The other two Lyapunov exponents are negative and larger in magnitude, than the first one. For parameter values  $L = 0.32$ ,  $\varepsilon = 0.02$  and  $m = 3$  (corresponding to Figures 6c,d) the Lyapunov exponents of attractor of Poincaré map are  $\Lambda = \{1.041 \pm 0.001, -3.860 \pm 0.001, -5.022 \pm 0.003\}$ . The first exponent is positive and close to the Lyapunov exponent of the Bernoulli map  $\Lambda_{B_3} = \ln 3 \approx 1.099$ . The other exponents are negative and larger in magnitude. The estimated Lyapunov exponents correspond to Smale – Williams type attractor with expansion factor  $m = 3$ .

The pivotal feature of uniformly hyperbolic attractors is transversality of stable and unstable manifolds<sup>38,39</sup>. To demonstrate this we calculate the distribution of angles between expanding and contracting subspaces of tangent bundle of sufficiently long trajectory of Poincaré map. We use the fast numerical algorithm<sup>40</sup>. Firstly, for a typical trajectory on the attractor, the linearized variation equations for the perturbation vector are solved to determine the expanding subspace (which is one-dimensional in our case). Points of trajectory and perturbation vectors  $\xi_n = [\delta x_n, \delta u_n, \delta y_n, \delta v_n]^T$  along it are stored in computer memory. Secondly, for the same trajectory in backward time we calculate the vectors orthogonal to the contracting subspace (which is two-

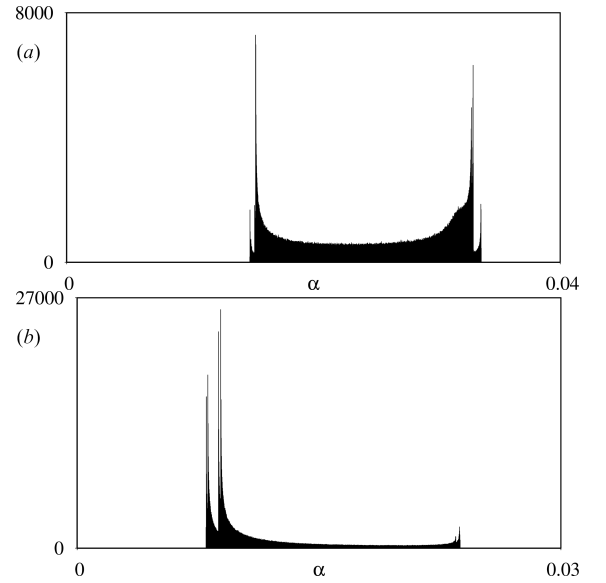


FIG. 7. Histograms of the angles of intersection of stable and unstable subspaces for the hyperbolic attractor of the Poincaré map of the system (12) at parameter values  $L = 0.32$ ,  $\varepsilon = 0.02$ . Panel (a) is for the system with expansion factor  $m = 2$ . Panel (b) is for  $m = 3$ .

dimensional in our case). The one way is to evaluate two senior perturbation vectors along the backward orbit using Gram – Schmidt orthogonalization and find orthogonal to them vector. Instead we calculate orthogonal complement vectors to the contracting subspaces directly by solving adjacent variation equations in backward time<sup>41</sup>. The vectors  $\eta_n = [\delta \tilde{x}_n, \delta \tilde{u}_n, \delta \tilde{y}_n, \delta \tilde{v}_n]$  orthogonal to contracting subspace are stored in computer memory along with perturbation vectors in forward time. Both sequences of vectors  $\{\xi_n\}$  and  $\{\eta_n\}$  lie on the Poincaré cross-section (vectors tangent to continuous trajectory  $[\dot{x}_n, \dot{u}_n, \dot{y}_n, \dot{v}_n]$  must be subtracted from  $\{\eta_n\}$  vectors for accuracy). At the end of the procedure, the angles are calculated through the scalar products of pairs of vectors:  $\alpha_n = \frac{\pi}{2} - \arccos \frac{\eta_n \cdot \xi_n}{\|\xi_n\| \|\eta_n\|}$ . The subtraction from  $\pi/2$  is required, because vectors  $\eta_n$  are orthogonal to the contracting subspaces. The sequence of angles  $\{\alpha_n\}$  is distributed on the interval  $[0, \pi/2]$ . The gist of the procedure described above is to ascertain the absence of zero angles.

Figures 7 show histograms of distributions of angles between expanding and contracting subspaces obtained numerically for the attractor of Poincaré map of the system (12) with  $m = 2$  and  $m = 3$  ( $L = 0.32$ ,  $\varepsilon = 0.02$ ). The interval  $[0, \pi/2]$  was split to  $10^5$  subintervals. The horizontal axis represents the amount of intersections between subspaces at given angle. The 1024 randomly chosen trajectories of the duration  $10^3$  (number of discrete time iterations) each were tested. For system with  $m = 2$  the minimal angle of intersection between subspaces is  $\alpha_{\min} = 0.01484402528821177 = 9.45 \cdot 10^{-3} \cdot \pi/2$ . For system with  $m = 3$  the minimal value of intersection an-

gles is  $\alpha_{\min} = 0.007995353303386023 = 5.09 \cdot 10^{-3} \cdot \pi/2$ . No intersection angles less than these values were found. Distribution edges break off sharply, no smooth decrease in the number of intersections towards zero angle is observed. The fact that the distributions are separated from zero, gives us strong confidence in the hyperbolic nature of the attractors. Nonetheless we are obliged to clarify, that our results are not a rigorous proof in the strict mathematical sense, since the technique is not supported by proved theorems. The implemented algorithm is able to clearly distinguish non-hyperbolic attractors as they have zero angles between subspaces, which are usually easy to find. The full computer-assisted proof is possible with sophisticated cone criteria.

Practically important feature of uniformly hyperbolic attractors is structural stability. Unlike quasiattractors, the Smale – Williams attractors occupy continuous domains in parameter space. We highlight such parameter domains by numerical plotting of Lyapunov exponents and expansion factor of angular variable, which is evaluated using the above algorithm. Fig. 8 show Lyapunov exponent dependencies on parameter  $L$ . Intervals with numerically recognized expanding solenoids are filled with yellow. On Fig. 8a the largest Lyapunov exponent (red line) approaches  $\ln 2$  value (green dash line) most closely inside the yellow-colored field (system with  $m = 2$ ). There is a domain of “smooth” Lyapunov exponents, the largest exponent does not fall to zero or negative values. We consider this a confirmation of robustness of chaotic attractor in a wide range of parameters. The regions of “smooth” exponents and factor 2 expansion do not coincide perfectly, the interval of robustness is wider than interval of confirmed attractors of Smale – Williams type. The residual “smooth” segments might be related to stages of attractor formation, but for now we reserve the study of these intriguing transitions to the investigations in future. The transition from periodic attractors to chaotic attractors (to the right of the domain of structurally stable chaotic regimes) is via period doubling cascade, which is typical for dissipative nonlinear systems. The estimated convergence constant to the accumulation point corresponds to Feigenbaum’s number  $\delta = 4.69 \dots$ . The transition to the left of the domain of structurally stable chaotic attractors is much more sharp and abrupt. The largest Lyapunov exponent on Fig. 8b (system with  $m = 3$ ) is very close to  $\ln 3$  on a wide interval. The domain of confirmed expanding solenoids is much larger then for the system with  $m = 2$ . The transition from periodic to chaotic attractors is via period doublings on both sides from the domain of structurally stable chaotic regimes.

Fig. 9 illustrates parameter spaces of system (12) with  $m = 2$  and 3. Regimes with solenoids (yellow color) occupy continuous domains, which is a feature of structurally stable attractors. Chaotic non-hyperbolic regimes (green color) separate domains of solenoids from stable periodic regimes (blue). Narrow windows of periodicity traverse regions of non-hyperbolic chaotic attractors. Red lines mark bifurcations of periodic cycles. No hyperchaotic (with two positive Lyapunov exponents) or quasiperiodic (with two zero Lyapunov exponents) are observed.

Fig. 10 shows attractors at different values of  $L$  (from 0.3

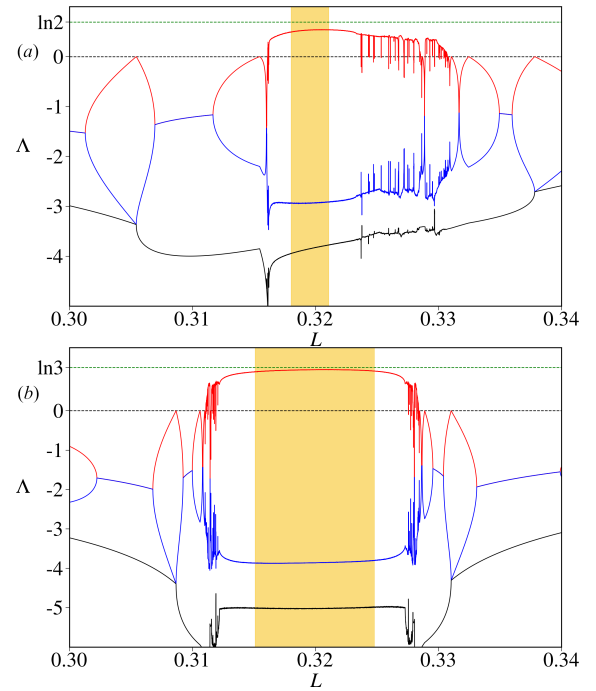


FIG. 8. Lyapunov exponents spectra vs. control parameter  $L$  for systems (12) Poincaré map. The value of  $\varepsilon$  is constant 0.02. The red graph is the largest Lyapunov exponent. The black dash line is zero level, the green dash line the level of  $\ln m$ . The yellow field corresponds to attractors with numerically calculated expansion factors  $m = 2$  and 3. Panel (a) is for the system with expansion factor  $m = 2$ . Panel (b) is for  $m = 3$ .

to 0.341) on the line  $\varepsilon = 0.04$  of atlas of regimes on Fig. 9a ( $m = 2$ ). Fig. 10(a) demonstrates the stable periodic cycle of period 2, projected onto the plane of variables  $(u_n, v_n)$ . Fig. 10(b) evidences multistability in the domain of periodic oscillations. Fig. 10(c) and (d) illustrate an example of non-hyperbolic chaotic attractor. One can observe pale part of attractor on (c) – this segment of attractor is visited rarely. Fig. 10(d) shows iterations of angular variable for the same attractor. One can see vertical segments, therefore the transformation of argument is discontinuous. Fig. 10(e) and (f) show the attractor, which we consider Smale – Williams type attractor, and iterations of angular variable, which we deem to be generated by Bernoulli-type mapping. Every part of narrow ring-shaped attractor is visited uniformly, larger value of  $\varepsilon$  (than for Fig. 5b) lets us see the glimpse of tight Cantor-like transverse structure, inherent to Smale – Williams attractor (at even larger  $\varepsilon$  one can see fractal structure with naked eye, but we prefer to keep  $\varepsilon$  small). Transformation of the angular variable is continuous, without gaps, segments with negative inclines or sharp vertical leaps. Fig. 10(g) and (h) demonstrate the non-hyperbolic attractor and the diagram for angular variable. Enlarged fragment shows “cut” or nonsmooth

This is the author's peer reviewed, accepted manuscript. However, the online version of record will be different from this version once it has been copyedited and typeset. PLEASE CITE THIS ARTICLE AS DOI: 10.1063/1.50028921

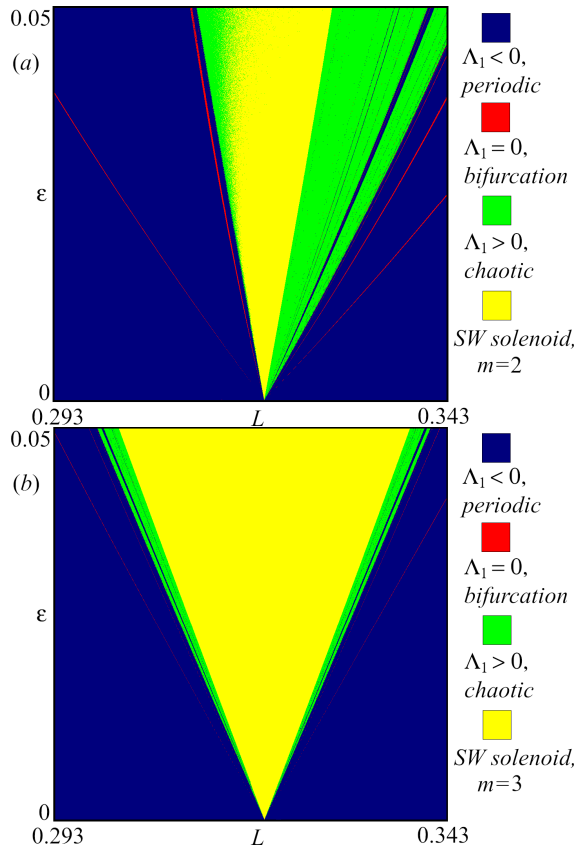


FIG. 9. Atlas of regimes, constructed by calculations of LEs and expansion factors for Poincaré map of (12). The yellow-colored dots correspond to solenoids with numerically calculated expansion factors  $m = 2$  and  $3$ . The green dots correspond to chaotic attractors, which are not solenoids. The blue dots are stable periodic regimes of different periods. Red-colored lines correspond to bifurcations of periodic cycles. Panel (a) is for the system with expansion factor  $m = 2$ . Panel (b) is for  $m = 3$ .

“bent” part of attractor. Transformation of angular variable has an interval with negative incline. Fig. 10(i) shows the non-hyperbolic attractor with gaps. Fig. 10(j) demonstrates two coexistent periodic attractors.

Fig. 11 shows attractors at different values of  $L$  (from 0.3 to 0.34) on the line  $\varepsilon = 0.04$  of atlas of regimes on Fig. 9b ( $m = 3$ ) and one example of Smale – Williams type attractor at higher value  $\varepsilon = 0.08$ . Fig. 11(a) demonstrates four stable periodic cycles of period 2, projected onto the plane of variables  $(u_n, v_n)$ . Fig. 11(b) shows two coexisting chaotic non-hyperbolic attractors. Fig. 11(c) and (d) illustrate an example of non-hyperbolic chaotic attractor. While Fig. 11(c) does not look suspicious, the panel (d) shows discontinuous transformation of angular variable with vertical segments. Fig. 11(e) and (f) demonstrate the attractor, which we con-

sider to be of Smale – Williams type, and iterations of angular variable. Transformation of the angular variable is three times, continuous, without gaps, segments with negative inclines or sharp vertical leaps. The scaled fragment shows, that three bands of attractor are close to each other in projection onto the plane  $(u_n, v_n)$ . To demonstrate the distinction between different bands we color them based on values of  $\arg w_{n-1} = \arg(u_{n-1} + iv_{n-1})$  from previous iterations. The green points are mapped from the interval  $[0, 2\pi/3)$ , red points are mapped from the interval  $[2\pi/3, 4\pi/3)$  and purple points are mapped from  $[4\pi/3, 2\pi)$ . It is possible to see gaps between bands at higher  $\varepsilon$  values (Fig. 11j). Fig. 11(g) and (h) demonstrate the non-hyperbolic attractor and the diagram for angular variable. Transformation of angular variable has sharp vertical leaps and negative incline segments close to them. Fig. 11(i) shows three stable periodic cycles.

The transitions from hyperbolic to non-hyperbolic attractors are observed via formations of vertical leaps or negative inclines on the diagrams for phases. Accurate quantitative investigations are required to give deeper description of bifurcations, leading to formation of the attractor of Smale – Williams type.

#### IV. SUMMARY

We have constructed an autonomous four-dimensional system of differential equations with attractors of apparently Smale – Williams type. The system is geometrically artificial and does not have a direct physical analog, but is very reminiscent of truncated equations, usually describing complex amplitudes of spatially distributed dynamical processes. In contrast with many previously known examples we have developed a consistent geometric approach, that illustrates the transformations in the phase space. The cornerstone of our model is the saddle equilibrium with two positive identical eigenvalues and two negative identical eigenvalues. Such equilibrium can be found in a system with two complex variables  $z$  and  $w$ . We have established a simple fact, that under a nonlinear perturbation  $\varepsilon w^m$  the transformation of the arguments of complex variables is  $m$  times expanding Bernoulli map in the small, but finite vicinity of the saddle. Therefore, one can construct a map from the neighborhood of the stable manifold of the saddle to the neighborhood of the unstable manifold of the saddle. The action of this map is generated by the flow of trajectories moving near the saddle. We have demonstrated via the perturbation analysis and with numerically obtained illustrations that an angular variable undergoes Bernoulli map. The Bernoulli map is an important part of transformations leading to the attractor of Smale – Williams type emergence. We have supplemented our construction with the mechanism of the return to the vicinity of the saddle. We have based additional nonlinear terms on the model with “figure-8” homoclinic trajectories of the saddle. Therefore we have obtained an attractor in the phase space of the flow.

We have investigated the chaotic attractor numerically. We have demonstrated in numerical simulations, that the Poincaré

This is the author's peer reviewed, accepted manuscript. However, the online version of record will be different from this version once it has been copyedited and typeset.  
PLEASE CITE THIS ARTICLE AS DOI: 10.1063/1.50028921

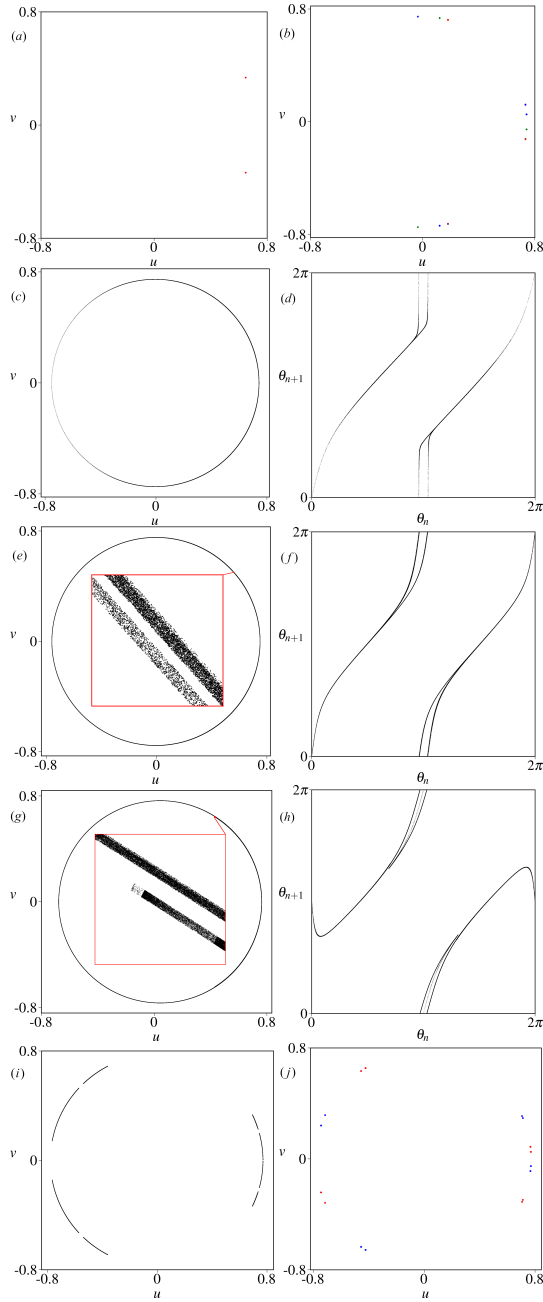


FIG. 10. Examples of attractors of Poincaré map of (11) with  $m = 2$ . Parameter  $\varepsilon = 0.04$  is the same for all examples, parameter  $L$  varies. Panel (a):  $L = 0.3$ , stable cycle of period 2; panel (b):  $L = 0.3127$ , three coexistent stable cycles of different periods; panels (c) and (d):  $L = 0.313$ , chaotic non-hyperbolic attractor and iterations of argument  $\theta$ ; panels (e) and (f):  $L = 0.32$ , Smale – Williams type attractor with scaled part and iterations of  $\theta$ ; panels (g) and (h):  $L = 0.33$ , chaotic non-hyperbolic attractor with scaled part and iterations of  $\theta$ ; panel (i):  $L = 0.34$ , chaotic non-hyperbolic attractor; panel (j):  $L = 0.341$ , two coexistent stable cycles of period 8.

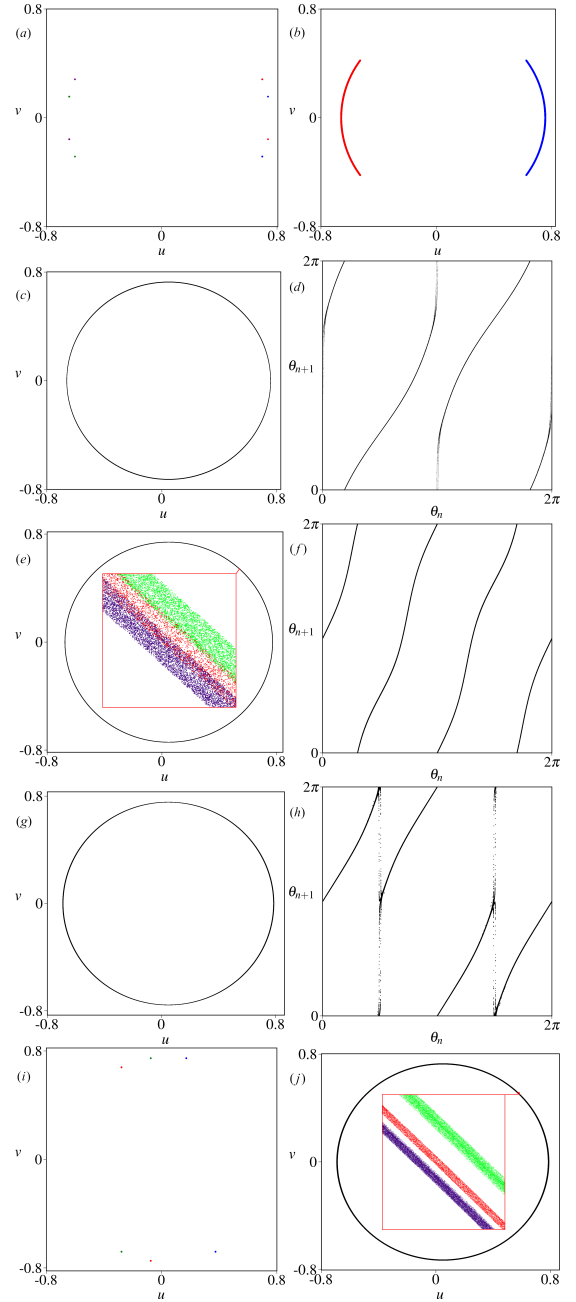


FIG. 11. Examples of attractors of Poincaré map of (12) with  $m = 3$ . Parameter  $\varepsilon = 0.04$  is the same for examples (a)-(i), parameter  $L$  varies. Panel (a):  $L = 0.302$ , four stable cycles of period 2; panel (b):  $L = 0.3035$ , two coexistent chaotic non-hyperbolic attractors; panels (c) and (d):  $L = 0.305$ , chaotic non-hyperbolic attractor and iterations of argument  $\theta$ ; panels (e) and (f):  $L = 0.32$ , Smale – Williams type attractor with scaled part and iterations of  $\theta$ , the colors correspond to different “branches” of the attractor; panels (g) and (h):  $L = 0.3347$ , chaotic non-hyperbolic attractor and iterations of  $\theta$ ; panel (i):  $L = 0.34$ , three stable cycles of period 2; panel (j):  $L = 0.32$ ,  $\varepsilon = 0.08$ , example of the Smale – Williams type attractor at higher  $\varepsilon$  and its scaled fragment, the colors mark different “loops” of the solenoid.

cross-section of the attractor corresponds to Smale – Williams type. Specifically, the angular variable, defined by the arguments of complex variables, undergoes  $m = 2, 3$  or  $4$  (see Appendix A) times expanding Bernoulli map (we have checked numerically the angular shift), while the attractor of the Poincaré map strongly shrinks in two other directions (we refer to the values of the corresponding negative Lyapunov exponents). We have verified the transversality of stable and unstable subspaces of the attractor with the angle criteria. We have observed the structural stability of attractor: the hyperbolic regime occupies a continuous domain of the parameter space. We also have glimpsed possible and numerically observable routes to destruction of the attractor of Smale – Williams type: when the transformation of the angular variable develops segments with negative incline or discontinuous segments in the form of vertical leaps. The underlying mechanisms of solenoid destruction in our model are unknown to us.

We consider our theory very general. In the process of preparing the manuscript we have found, that the same construction underlies the formation of Smale – Williams attractor in previously studied autonomous spatially distributed model<sup>23</sup>. The referred system is modified Swift – Hohenberg equation, the well-known in pattern formation studies<sup>42</sup>, with periodic spatial inhomogeneity and an additional variable. The finite-dimensional approximation with complex amplitude equations, describing the most important spatial modes, has a saddle equilibrium, with trajectories “scattering” on it by the map of Bernoulli type with factor  $m = -2$ . Interestingly, the dynamics of linear approximation in the vicinity of the saddle has diagonal Jacobi matrix. The return mechanism differs from one reported here. These results will be developed elsewhere.

We are interested in uncovering the connections between the present report and previous results on autonomous systems with hyperbolic attractors<sup>21</sup>, where the model with saddle-focus (two conjugated eigenvalues with positive real part and two conjugated eigenvalues with negative real part) instead of saddle was proposed. Three models with heteroclinic cycles of saddle limit cycles, with hyperbolic attractors in their vicinity, were also proposed<sup>21</sup>. At present, we do not know if it is possible to introduce the imaginary parts of eigenvalues, such that the saddle becomes the saddle-focus, without the violation of the mechanisms described by us. We are also interested in development of the similar approach for nonautonomous dynamical systems with Smale – Williams attractors<sup>43</sup>.

The provided results are numerical, but we hope that our approach might lead to physically valid models with rigorous analytical proofs of Smale – Williams attractor existence.

#### ACKNOWLEDGMENTS

The work was performed in the framework of a state task to the Kotelnikov Institute of Radioengineering and Electronics of Russian Academy of Sciences. The authors thank A. Kazakov, P. Kuptsov and A. Rozhnev for useful discussions.

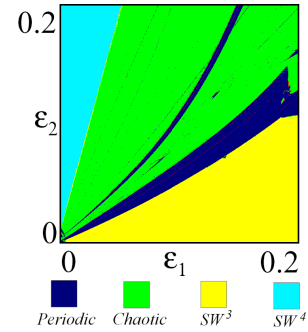


FIG. 12. Atlas of regimes, constructed by calculations of LEs and expansion factors for Poincaré map of (A1). The yellow-colored dots correspond to solenoids with numerically calculated expansion factors  $m = 3$  and cyan-colored dots correspond to solenoids with  $m = 4$ . The green dots correspond to chaotic attractors, which are not solenoids. The blue dots are stable periodic regimes of different periods. Red-colored lines correspond to bifurcations of periodic cycles.

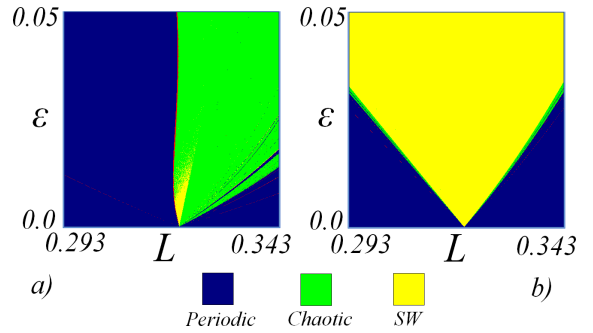


FIG. 13. Atlases of regimes, constructed by calculations of LEs and expansion factors for Poincaré map of the systems (A2) and (A3). The yellow-colored dots correspond to solenoids with numerically calculated expansion factor  $m = 2$ . The green dots correspond to non-hyperbolic chaotic attractors. The blue dots are stable periodic regimes of different periods. Red-colored lines correspond to bifurcations of periodic cycles. Panel (a) is for the system (A2). Panel (b) is for (A3).

*The data that support the findings of this study (computer programs, pictures) are available from the authors upon reasonable request.*

#### Appendix A: Different variants of perturbations of trajectories near the saddle equilibria

The structural stability means not only the insensitivity of attractor structure to parameter variations, but the qualitative preservation of behaviour, if the functions in governing equations are changed. The perturbation force can be polynomial

of  $w$ :

$$\begin{aligned} \dot{z} &= w, \\ \dot{w} &= (1 - |z|^2)z + [L - (1 - |z|^2)^2]w + \varepsilon_1 w^3 + \varepsilon_2 w^4. \end{aligned} \quad (\text{A1})$$

In this modified system the perturbation has two terms of order 3 and 4. We have found, that model (A1) manifests two topological types of solenoids with expansion factors  $m = 3$  and  $m = 4$  at different parameter ranges. Fig. 12 shows atlas of regimes of Poincaré map of the system (A1) (the cross-section is  $|z|^2 = 1$  as before). The technique is the same as for Fig. 9. Yellow domain corresponds to solenoids with expansion factor  $m = 3$ , cyan domain corresponds to solenoids with  $m = 4$ . There are non-hyperbolic regimes between these regions.

We have also studied briefly the variants of the model with perturbation forces  $\varepsilon z^2$ :

$$\begin{aligned} \dot{z} &= w, \\ \dot{w} &= (1 - |z|^2)z + [L - (1 - |z|^2)^2]w + \varepsilon z^2, \end{aligned} \quad (\text{A2})$$

and with  $\varepsilon zw$ :

$$\begin{aligned} \dot{z} &= w, \\ \dot{w} &= (1 - |z|^2)z + [L - (1 - |z|^2)^2]w + \varepsilon zw. \end{aligned} \quad (\text{A3})$$

We doubt the existence of attractors of Smale – Williams type in the system (A2). It does not have a continuum circle of equilibria, like the system (12). Recall, that trajectories of flow system (12) revolve around points of equilibria ( $e^{i\varphi}, 0$ ) in such way, that the arguments of complex variables do not change (when they are far from the saddle). We have found very small region of parameters of (A2), where the numerically calculated expansion factor is equal to 2. The system (A3) has the continuum of equilibria ( $e^{i\varphi}, 0$ ), solenoids appear in its Poincaré cross-section very similar to the system (12). Fig 13 shows atlases of regimes for systems (A2) and (A3).

#### Appendix B: The system based on one-sided homoclinic loop

The existence of a homoclinic “figure-8” bifurcation in the system is not a necessary condition for the emergence of the attractor of Smale – Williams type. Let’s discuss the system of real-valued variables

$$\begin{aligned} \dot{x} &= u, \\ \dot{u} &= (1 - x)x + [L - (1 - x)^2]u. \end{aligned} \quad (\text{B1})$$

It is very similar to oscillator model (9), but instead of two-sided homoclinic loop it manifests one-sided homoclinic loop at  $L \approx 0.14521$  (see Fig. 14).

We repeat the steps from the section II and derive the four-dimensional system with complex variables:

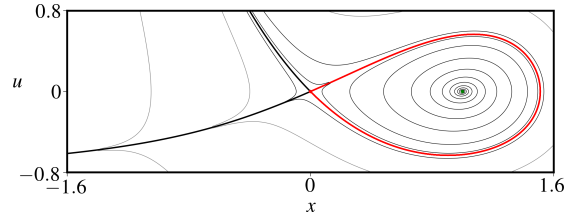


FIG. 14. Numerical solutions of equations (B1).  $L \approx 0.14521$ . The limit cycle is colored red, saddle equilibrium is pointed red, focus is pointed green.

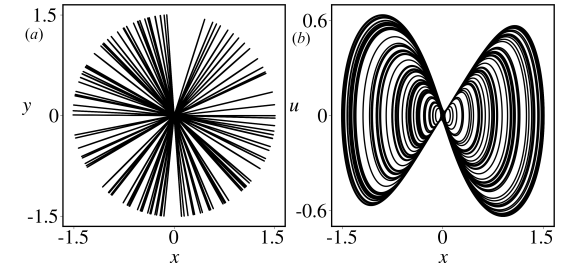


FIG. 15. Projections of attractor in flow system (B2) on the plane of variables  $x = \text{Re } z$  and  $y = \text{Im } z$ , panel (a), on the plane of variables  $x = \text{Re } z$  and  $u = \text{Im } z$ , panel (b),  $L = 0.143$ ,  $\varepsilon = 0.02$ ,  $m = 3$ .

$$\begin{aligned} \dot{z} &= w, \\ \dot{w} &= (1 - |z|)z + [L - (1 - |z|)^2]w + \varepsilon w^m, \end{aligned} \quad (\text{B2})$$

now absolute values  $|z|$  are not squared. The dynamics of model is nevertheless very similar to (12). Fig. 15 shows the attractor of the flow system (B2) at  $L = 0.143$ ,  $\varepsilon = 0.02$  with expansion factor  $m = 3$ . The attractor is very similar to the attractor on the Fig. 4. The trajectories move very close to one-sided loop, while revolving around the points of the continuum of equilibria. Near the saddle the trajectories “scatter” with different angle (under Bernoulli-type map), therefore the two-dimensional projection looks like fitted inside “figure-8” loop. Fig. 16 demonstrate the iterations of angular variable  $\theta = \arg z$  and the attractor projected onto the plane of variables  $u = \text{Re } w$ ,  $v = \text{Im } w$  in Poincaré cross-section by  $|z|^2 = 1$ . The transformation of the angular variable is three times expanding Bernoulli-type map. Fig. 17 shows atlas of regimes of the system (B2) with  $m = 3$ . The domain of solenoids is continuous, as it should be for structurally stable regimes.

<sup>1</sup>L. Shil’nikov and D. Turaev, “Simple bifurcations leading to hyperbolic attractors,” *Computers & Mathematics with Applications* **34**, 173–193 (1997).

<sup>2</sup>D. Turaev and L. Shil’nikov, “Blue sky catastrophes,” in *DOKLADY MATHEMATICS C/C OF DOKLADY-AKADEMIIA NAUK*, Vol. 51 (MAIK NAUKA, 1995) pp. 404–407.

<sup>3</sup>D. V. Anosov, “Dynamical systems in the 1960s: the hyperbolic revolution,” in *Mathematical events of the twentieth century* (Springer, 2006) pp. 1–17.

<sup>4</sup>S. Smale, “Differentiable dynamical systems,” *Bulletin of the American mathematical Society* **73**, 747–817 (1967).

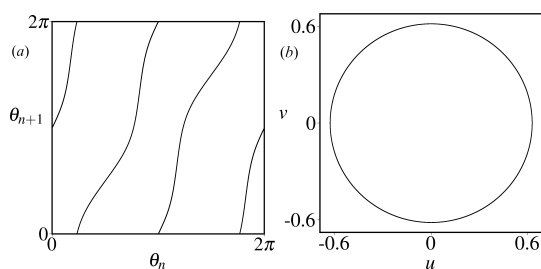


FIG. 16. Iterations of argument  $\theta_{n+1}$  vs.  $\theta_n$  (a) and the attractor of Poincaré map (b) of the system (B2),  $L = 0.143$ ,  $\varepsilon = 0.02$ ,  $m = 3$ .

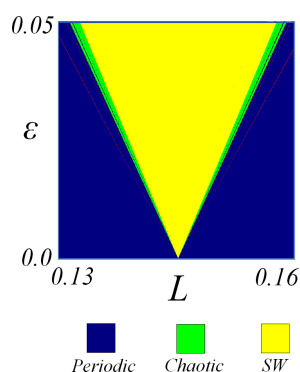


FIG. 17. Atlas of regimes, constructed by calculations of LEs and expansion factors for Poincaré map of (B2). The yellow-colored dots correspond to solenoids with numerically calculated expansion factors  $m = 3$  and cyan-colored dots correspond to solenoids with  $m = 4$ . The green dots correspond to chaotic attractors, which are not solenoids. The blue dots are stable periodic regimes of different periods. Red-colored lines correspond to bifurcations of periodic cycles.

- <sup>5</sup>D. Anosov, G. Gould, S. Aranson, V. Grines, R. Plykin, A. Safonov, E. Sataev, S. Shlyachkov, V. Solodov, A. Starkov, *et al.*, *Dynamical systems IX: dynamical systems with hyperbolic behaviour* (Springer, 1995).
- <sup>6</sup>A. Katok and B. Hasselblatt, *Introduction to the modern theory of dynamical systems*, Vol. 54 (Cambridge university press, 1997).
- <sup>7</sup>L. P. Shilnikov, "Mathematical problems of nonlinear dynamics: A tutorial," *International Journal of Bifurcation and Chaos* **7**, 1953–2001 (1997).
- <sup>8</sup>S. P. Kuznetsov, "Dynamical chaos and uniformly hyperbolic attractors: from mathematics to physics," *Physics-Uspokhi* **54**, 119 (2011).
- <sup>9</sup>S. P. Kuznetsov, *Hyperbolic Chaos: A Physicist's View* (Higher Education Press: Beijing and Springer, 2012).
- <sup>10</sup>V. S. Afraimovich and S. L. P. "Strange attractors and quasi-attractors," in *Nonlinear Dynamics and Turbulence*, eds. Barenblatt, G. I., Iooss, G. and Joseph, D. D. (Pitman, New York, 1983) pp. 1–28.
- <sup>11</sup>A. S. Gonchenko, S. V. Gonchenko, A. O. Kazakov, and A. Kozlov, "Elements of contemporary theory of dynamical chaos: a tutorial. part i. pseudohyperbolic attractors," *International Journal of Bifurcation and Chaos* **28**, 1830036 (2018).
- <sup>12</sup>D. V. Turaev and L. P. Shil'nikov, "An example of a wild strange attractor," *Sbornik: Mathematics* **189**, 291 (1998).
- <sup>13</sup>V. S. Afraimovich, V. Bykov, and L. P. Shilnikov, "On the origin and structure of the lorenz attractor," *DoSSR* **234**, 336–339 (1977).
- <sup>14</sup>J. Guckenheimer and R. F. Williams, "Structural stability of lorenz attractors," *Publications Mathématiques de l'Institut des Hautes Études Sci-*

- tiques* **50**, 59–72 (1979).
- <sup>15</sup>L. Shilnikov, "Bifurcations and strange attractors," arXiv preprint math/0304457 (2003).
- <sup>16</sup>R. Barrio, A. Shilnikov, and L. Shilnikov, "Kneadings, symbolic dynamics and painting lorenz chaos," *International Journal of Bifurcation and Chaos* **22**, 1230016 (2012).
- <sup>17</sup>T. Xing, R. Barrio, and A. Shilnikov, "Symbolic quest into homoclinic chaos," *International Journal of Bifurcation and Chaos* **24**, 1440004 (2014).
- <sup>18</sup>E. N. Lorenz, "Deterministic nonperiodic flow," *Journal of the atmospheric sciences* **20**, 130–141 (1963).
- <sup>19</sup>R. F. Williams, "Expanding attractors," *Publications Mathématiques de l'Institut des Hautes Études Scientifiques* **43**, 169–203 (1974).
- <sup>20</sup>S. P. Kuznetsov, "Example of a physical system with a hyperbolic attractor of the smale – williams type," *Physical review letters* **95**, 144101 (2005).
- <sup>21</sup>S. P. Kuznetsov and A. Pikovsky, "Autonomous coupled oscillators with hyperbolic strange attractors," *Physica D: Nonlinear Phenomena* **232**, 87–102 (2007).
- <sup>22</sup>V. Kruglov and S. Kuznetsov, "An autonomous system with attractor of smale – williams type with resonance transfer of excitation in a ring array of van der pol oscillators," *Communications in Nonlinear Science and Numerical Simulation* **16**, 3219–3223 (2011).
- <sup>23</sup>V. P. Kruglov, S. P. Kuznetsov, and A. Pikovsky, "Attractor of smale-williams type in an autonomous distributed system," *Regular and Chaotic Dynamics* **19**, 483–494 (2014).
- <sup>24</sup>S. P. Kuznetsov and I. R. Sataev, "Hyperbolic attractor in a system of coupled non-autonomous van der pol oscillators: Numerical test for expanding and contracting cones," *Physics Letters A* **365**, 97–104 (2007).
- <sup>25</sup>D. Wilczak, "Uniformly hyperbolic attractor of the smale–williams type for a poincaré map in the kuznetsov system," *SIAM Journal on Applied Dynamical Systems* **9**, 1263–1283 (2010).
- <sup>26</sup>S. Kuznetsov and E. Seleznev, "A strange attractor of the smale-williams type in the chaotic dynamics of a physical system," *Journal of Experimental and Theoretical Physics* **102**, 355–364 (2006).
- <sup>27</sup>L. P. Shilnikov, "On the generation of a periodic motion from trajectories doubly asymptotic to an equilibrium state of saddle type," *Matematicheskii Sbornik* **119**, 461–472 (1968).
- <sup>28</sup>The eigenvectors that span the plane tangent to the stable manifold are  $\hat{e}_1 \approx [-0.58227883, 0.81298916, 0, 0]^T$  and  $\hat{e}_2 \approx [0, 0, -0.58227883, 0.81298916]^T$  at  $a = -0.68$ . The initial conditions close to the stable manifold were picked  $z(0) = -0.58227883 \exp i\theta$ ,  $w(0) = 0.81298916 \exp i\theta$ . There were overall 4096 trajectories with initial angles  $\theta$  evenly distributed. The numerical integration of the particular trajectory stopped, when  $|z|$  exceeded 1.
- <sup>29</sup>I. S. Aranson and L. Kramer, "The world of the complex ginzburg – landau equation," *Reviews of modern physics* **74**, 99 (2002).
- <sup>30</sup>V. P. Kruglov and L.-B. Khadzheva, "Uniformly hyperbolic attractor in a system based on coupled oscillators with «figure-eight» separatrix," *Izvestiya VUZ. Applied Nonlinear Dynamics* **24**, 54–64 (2016).
- <sup>31</sup>S. P. Kuznetsov and Y. V. Sedova, "Hyperbolic chaos in the bonhoeffer–van der pol oscillator with additional delayed feedback and periodically modulated excitation parameter," *Izvestiya VUZ. Appl. Nonlin. Dyn* **27**, 77–95 (2019).
- <sup>32</sup>S. P. Kuznetsov and Y. V. Sedova, "Robust hyperbolic chaos in froude pendulum with delayed feedback and periodic braking," *International Journal of Bifurcation and Chaos* **29**, 1930035 (2019).
- <sup>33</sup>S. Kuznetsov, V. Kruglov, and Y. Sedova, "Mechanical systems with hyperbolic chaotic attractors based on froude pendulums," *Russian Journal of Nonlinear Dynamics* **16**, 51–58 (2020).
- <sup>34</sup>G. Benettin, L. Galgani, A. Giorgilli, and J.-M. Strelcyn, "Lyapunov characteristic exponents for smooth dynamical systems and for hamiltonian systems: a method for computing all of them. part 1: Theory," *Meccanica* **15**, 9–20 (1980).
- <sup>35</sup>I. Shimada and T. Nagashima, "A numerical approach to ergodic problem of dissipative dynamical systems," *Progress of theoretical physics* **61**, 1605–1616 (1979).
- <sup>36</sup>A. Pikovsky and A. Politi, *Lyapunov exponents: a tool to explore complex dynamics* (Cambridge University Press, 2016).
- <sup>37</sup>The orthogonalizations were performed with DGEQRF and DORGQR routines from LAPACK library. LEs were calculated for  $10^3$  randomly selected trajectories, the provided results are average values of LEs and standard de-

- viations. Values were rounded to the first significant digits of deviations.
- <sup>38</sup>Y.-C. Lai, C. Grebogi, J. Yorke, and I. Kan, "How often are chaotic saddles nonhyperbolic?" *Nonlinearity* **6**, 779 (1993).
- <sup>39</sup>V. S. Anishchenko, A. Kopeikin, J. Kurths, T. Vadivasova, and G. Strelkova, "Studying hyperbolicity in chaotic systems," *Physics Letters A* **270**, 301–307 (2000).
- <sup>40</sup>P. V. Kuptsov, "Fast numerical test of hyperbolic chaos," *Physical Review E* **85**, 015203 (2012).
- <sup>41</sup>Adjacent equations are such that the Jacobi matrix of evolution operator is conjugate transposed and all of its elements are multiplied by  $-1$ . The rea-

- son of using the conjugate transposed matrix is that its eigenvectors are orthogonal to eigenvectors (with eigenvalues not conjugate transpose of each other) of original matrix. One can also calculate the Lyapunov exponent corresponding to perturbation vector in forward time and Lyapunov exponent of adjacent perturbation vector in backward time and see, that they converge to the same value.
- <sup>42</sup>M. C. Cross and P. C. Hohenberg, "Pattern formation outside of equilibrium," *Reviews of modern physics* **65**, 851 (1993).
- <sup>43</sup>L. Turukina and A. Pikovsky, "Hyperbolic chaos in a system of resonantly coupled weakly nonlinear oscillators," *Physics Letters A* **375**, 1407–1411 (2011).

This is the author's peer reviewed, accepted manuscript. However, the online version of record will be different from this version once it has been copyedited and typeset.  
PLEASE CITE THIS ARTICLE AS DOI: 10.1063/1.50028921